Research Article | Vol. 30, No. 15 / 18 Jul 2022 / Optics Express 26229
Optics EXPRESS

Direct nanoimprint of chalcogenide glasses with optical functionalities via solvent-based surface softening

SIVAN TZADKA SHALIT,[1,2] NATALI OSTROVSKY,[1,2] HADAR FRANKENSTEIN SHEFA,[3] EVYATAR KASSIS,[3] SHAY JOSEPH,[3] AND MARK SCHVARTZMAN[1,2,*]

[1]*Department of Materials Engineering, Ben-Gurion University of the Negev, Beer-Sheva, Israel*
[2]*Ilse Katz Institute for Nanoscale Science and Technology, Ben-Gurion University of the Negev, Beer-Sheva, Israel*
[3]*Optical Component Center, Rafael Advanced Defense Systems, Haifa, Israel*
[*]*marksc@bgu.ac.il*

Abstract: Chalcogenide glasses are attractive materials for optical applications. However, these applications often require patterning of the surface with functional micro-/ nanostructures. Such patterning is challenging by traditional microfabrication methods. Here, we present a new, to the best of our knowledge, approach of direct imprint via solvent-based surface softening, for the patterning of As_2Se_3 surface. Our approach is based on an elastomeric stamp soaked in an organic solvent. During the imprint, the solvent diffuses into the imprinted substrate, plasticizes its surface, and thereby allows its imprint at the temperature below its glass transition point. Thus, our approach combines the full pattern transfer with the maintenance of the shape of the imprinted substrate, which is necessary for optical devices. By using this approach, we demonstrated functional antireflective microstructures directly imprinted on As_2Se_3 surface. Furthermore, we showed that our approach can produce imprinted features sized down to 20 nm scale. We believe that our new approach paves the way for more future applications of chalcogenide glasses.

Chalcogenide glasses are attractive optical materials [1–3] due to their high near- and mid-infrared transmission and refractive index, which can be modified by varying the glass composition [4]. In addition, chalcogenide glasses overcome phase transition upon interaction with electrons, X-rays, and photons [5,6], which makes them attractive materials for non-volatile memory devices [7]. Furthermore, chalcogenide glasses demonstrate third-order non-linearity, which stems from the low phonon energy of the bonds connecting the heavy chalcogenide atoms, making them attractive for optical switching applications [8]. Finally, chalcogenide glasses have relatively low glass transition temperature (T_g), which ranges between 150°C and 200°C, depending on the glass composition [9]. Such low T_g enables scalable and cost-effective fabrication of optical components using precision glass molding [10]. These unique properties make chalcogenide glasses advantageous over other materials commonly used in infrared optics, such as silicon or germanium whose applications in optical components such as windows or lenses require expensive and complicated processing based on grinding and precision polishing.

Despite numerous advantages of chalcogenide glasses, their practical application in optical devices is still challenging. Bare chalcogenide glasses reflect more than 20% of light in the infrared spectrum, therefore, their surface must be covered with an antireflective coating. Classical antireflective coatings based on vacuum-deposited films have low compatibility with chalcogenide glasses due to the difficulty in the index matching of the deposited films, poor adhesion of these films to the surface of chalcogenide glass, and relatively high mismatch between the thermal expansion coefficients of chalcogenide glasses and those of antireflective films. The latter often results in cracking and mechanical delamination of the deposited films, which in turn substantially

#462448 https://doi.org/10.1364/OE.462448
Journal © 2022 Received 27 Apr 2022; revised 18 May 2022; accepted 18 May 2022; published 5 Jul 2022

Optics EXPRESS

hampers their antireflective performance. Furthermore, thin-film-based antireflective coatings are effective only for a limited range of wavelengths and incident angles, which limits their use for broadband applications.

An emerging alternative to thin-film-derived antireflective nanostructures is based on microfabricated arrays of subwavelength 3D structures, whose concept was inspired by natural subwavelength structures discovered on the cornea of nocturnal moth *Spodoptera eridania* [11]. Today, such nanostructures can be fabricated on optical surfaces using standard nanofabrication techniques, and their periodicity and geometry can be tailored to achieve broadband and omnidirectional antireflective performance that is hardly achievable by thin-film based coating [12]. Whilst the fabrication of antireflective subwavelength structures was successfully demonstrated on commonly used optical materials such as glass, quartz, or Si [13,14], their fabrication of chalcogenide glasses still requires a new, and unconventional approach suited explicitly for this family of materials.

Soft thermal imprinting is an attractive approach for the surface micro-structuring of chalcogenide glasses. As already mentioned above, chalcogenide glasses can be imprinted due to their low glass transition temperature. Up to date, soft imprinting was successfully demonstrated on thin films of chalcogenide glasses deposited on solid substrates [15–18]. In such an imprint, which is schematically shown in Fig. 1(a), a pattern can be transferred from an elastomeric mold to the surface of the chalcogenide film, which is softened due to the heating above its glass transition point, whereas the underlying solid substrate made of silicon for example, remains undeformed. This approach, however, is inapplicable for the direct surface patterning of substrates made of chalcogenide glass. Indeed, the combination of high pressure and temperature needed to transfer a pattern from a mold to the surface of chalcogenide glass would also deform the substrate itself, making it inapplicable as a component for precision refractive optics (Fig. 1(b)). On the other hand, low pressure and temperature imprinting would result only in partial pattern transfer [19] (Fig. 1(c)). Ideally, the imprint should result in a full pattern transfer while maintaining the original shape of the substrate (Fig. 1(d)).

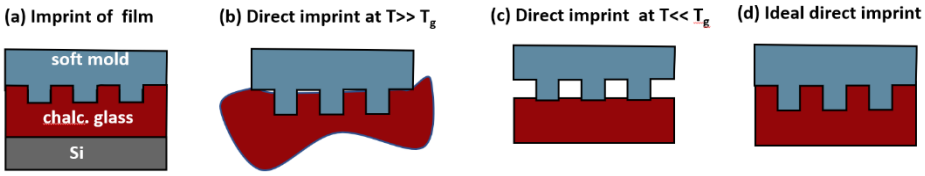

Fig. 1. Various concepts of nanoimprint of chalcogenide glasses.

Several approaches for the direct imprint on chalcogenide glasses have been recently suggested. One such approach is based on confining a substrate of chalcogenide-glass within a tight metallic fixture that prevents the substrate deformation during the imprinting [20–23]. Yet, this approach requires custom-made fixtures for each substrate geometry. Furthermore, the maintenance of the original substrate shape was never quantified for this method of imprinting. Two other approaches were recently demonstrated by our group. The first one was based on the radiative imprinting with a carbon-nanotube (CNT) reinforced Polydimethylsiloxane (PDMS) mold [24]. Due to the light absorbance of CNT-PDMS mold, only the mold-glass interface is heated and imprinted, while the bulk of the imprinted substrate is kept below its glass transition temperature, and therefore remains undeformed. However, the complex preparation of nanotube-PDMS composite mold substantially complicates this fabrication approach. Another approach was based on the imprinting of a plasticized film of chalcogenide glass deposited from solution onto a chalcogenide-glass substrate, which can be done at a temperature below the glass transition point of the substrate [25]. However, this process is challenging due to the difficulty of controlling the

Optics EXPRESS

thickness of the plasticized film, especially for films with submicron thicknesses. Thus, facile, robust, and versatile approaches for the direct surface imprint of chalcogenide glasses are still to be explored. Once developed, such approaches will pave the way to numerous optical applications of chalcogenide glasses that require their surface patterning, including but not limited to the production of antireflective structures.

This work introduces a novel approach for the direct surface patterning of chalcogenide glasses, which is based on their imprinting with a PDMS-based mold. The key feature of this approach, which is schematically described in Fig. 2(a), is the soaking of PDMS mold in a solvent capable of dissolving the imprinted chalcogenide glass. While soaked for a controlled time, the mold turns into a reservoir of a controlled amount of the solvent. The mold is then immediately used for the imprinting, during which the solvent partially diffuses from the mold into the glass and softens its surface. In this way, the surface can be imprinted at a temperature lower than the glass transition point of the pristine chalcogenide glass. In this case, the pattern is fully transferred from the mold to the softened surface, while the deformation of the bulk of the imprinted glass is completely avoided. We successfully applied this approach to produce various micro-/nanopatterns. First, we demonstrated that despite the relative simplicity of this imprinting approach, it could be used to replicate features as small as 20 nm. We then investigated the chemical composition and structure of the imprinted surface and concluded that they do not differ from those of pristine chalcogenide glass. This important conclusion supported the idea that this novel approach can be used to directly pattern optical functionalities on the surface of chalcogenide glass, whilst the functionalities and the underlying surface can be designed with the same optical properties. We implemented this idea by directly imprinting fully functional moth eye antireflective structures that yield an excellent broadband and omnidirectional attenuation of surface reflection in the infrared spectrum. Thereby, we demonstrated the applicability of our imprinting approach to produce miniaturized structures with a broad range of size scales and functionalities.

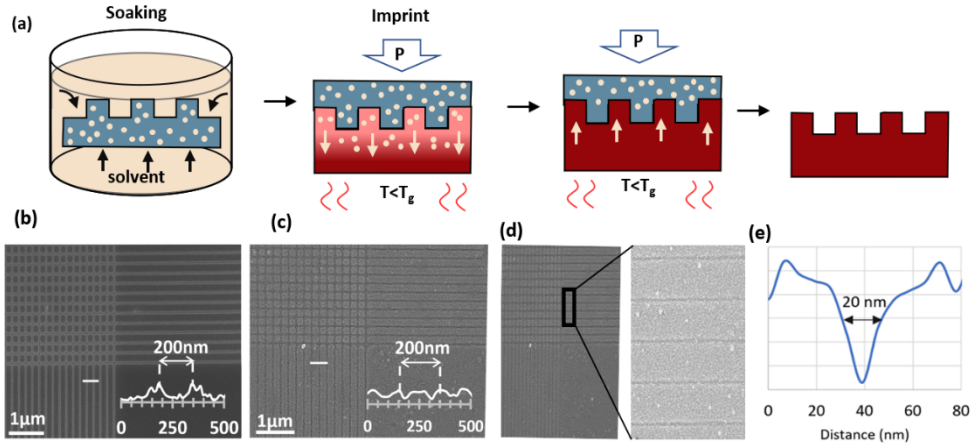

Fig. 2. (a) Schematic pross flow of direct imprint of As_2Se_3 substrate. (b),(c) SEM images of 2D grating in master mold and on the surface of the imprinted As_2Se_3, respectively. (d) High-magnification SEM of the grating on As_2Se_3. (e) Cross section profile of the imprinted line showing its FWHM.

First, we explored the limits of our imprint approach to replicate ultra-small features. To that end, we produced a master mold by patterning arrays of 20 nm lines in a positive-tone electron-beam resist (PMMA) on a silicon substrate (Fig. 2(b)) and used it for direct replication of PDMS-based soft mold. The mold itself consisted of an imaging hard-PDMS layer and soft PDMS – a configuration that ensures a reliable transfer of such ultra-small features [26]. To produce

Optics EXPRESS

1" As_2Se_3 substrates, we first mixed As and Se in stoichiometric proportions inside a quartz ampoule, fussed the mixture under vacuum, quenched it in air, and molded the obtained glass in a dedicated preform. Prior to the imprinting, the mold was soaked for 5 min in ethylenediamine (EDA), an organic solvent capable of dissolving As_2Se_3. Then, the mold was immediately apposed on the As_2Se_3 substrate in a custom-made nanoimprinting tool by applying a pneumatic pressure of 4 bar and a temperature of 165°C for 30 min. At the end of the imprinting process, the substrate and the mold were cooled down to ambient temperature, the pressure was released, and the mold was gently peeled off the substrate.

Figure 2(c) shows SEM images of a 2D array of 20 nm lines imprinted on the surface of As_2Se_3. Visual inspection of these lines, and their comparison to the original lines patterned on the master mold, clearly demonstrate that the pattern was transferred with high fidelity. This fidelity can be further quantified by measuring the full-width half-maximum (FWHM) of the cross-section profile for imprinted lines (Figs. 2(d) and (e)). Furthermore, the periodicity of the lines in the master mold was 200 nm, and the exact same periodicity was found for the imprinted pattern (insets in Figs. 2(b) and (c)). These data confirm that nanometric patterns imprinted by our approach are transferred with a very high fidelity and that the possible effect of the PDMS volume expansion due to EDA absorption on the obtained pattern geometry was negligible.

It should be noted that the demonstrated pattern was imprinted at a temperature below that of the glass transition point of As_2Se_3. This low imprint temperature was possible due to the softening of the surface layer of the imprinted glass by the EDA. A similar solvent-diffusion-based imprint was recently demonstrated by us using polymeric substrates, where the thickness of the softened layer was estimated by diffusion modeling to be around a few microns [27]. Similar to the mechanism of solvent-assisted polymer imprint, here it can be hypothesized that at later stages of the imprinting, a great portion of EDA molecules diffuse out of the mold. This diffusion likely produces a negative gradient in the EDA concentration between the imprinted glass and the mold. This gradient drives a backward migration of EDA molecules from the imprinted glass to the mold. Also, a part of EDA diffuses from the surface into the bulk. These two possible mechanisms of EDA loss from the imprinted surface layer at the late stage of the process cause the transition of the imprinted layer from a softened state to the solid amorphous As_2Se_3, which is similar by composition and properties to that of pristine As_2Se_3. In the context of the optical application of our imprinting process, it is crucial to verify that the interaction of the mold with the imprinted glass does not alter the composition of the latter in a way that can negatively affect its optical properties [28]. For that purpose, we first compared the compositions of the bare and imprinted As_2Se_3 surfaces using X-ray photoelectron spectroscopy (XPS), focusing on the ratio between As and Se atoms (Figs. 3(a),(b)). We found that As/Se ratio was nearly the same throughout the processing steps, with an average value of around 0.71. An additional important aspect of the chemical composition of imprinted As_2Se_3 are possible solvent residuals, which must be minimized. EDA, which was used in this work as the solvent, contains only carbon, nitrogen, and hydrogen. However, neither carbon nor nitrogen can be quantitatively measured by XPS, because the C*-N peak at 286 eV, which is a common surface marker for nitrogen-containing organic molecules, overlaps with the Auger peak of Se, and N*-C peak at 400 eV overlaps with the LM5 peak of Se. As an alternative to XPS, we used energy dispersive spectroscopy (EDS) to quantify the nitrogen content. Figure 3(c) shows the EDS data for nitrogen and oxygen content on the surface of bare and imprinted As_2Se_3. It can be seen that bare As_2Se_3 contains no nitrogen at all. However, imprinted As_2Se_3 contains about 5% nitrogen which can be attributed to residuals of EDA. Also, a high oxygen content on the surface of As_2Se_3 can be attributed to contamination. Since this amount of oxygen is nearly the same as on the imprinted surface, it can be concluded that the imprint process did not lead to the oxidation of As_2Se_3 because the imprinting took place in vacuum. One possible negative side-effect of thermal processing of chalcogenide glasses is the crystallization of their surfaces, which can hinder their

Optics EXPRESS

optical transparency by light scattering [18]. To test whether our imprinting process causes any crystallization of As_2Se_3, we characterized the imprinted surface by X-ray electron diffraction ($\lambda_{CuK\alpha} = 0.1542$ nm) (Fig. 3(d)). The measured spectrum shows broad peaks characteristic of amorphous As_2Se_3, and clearly demonstrates that our process does not induce crystallization.

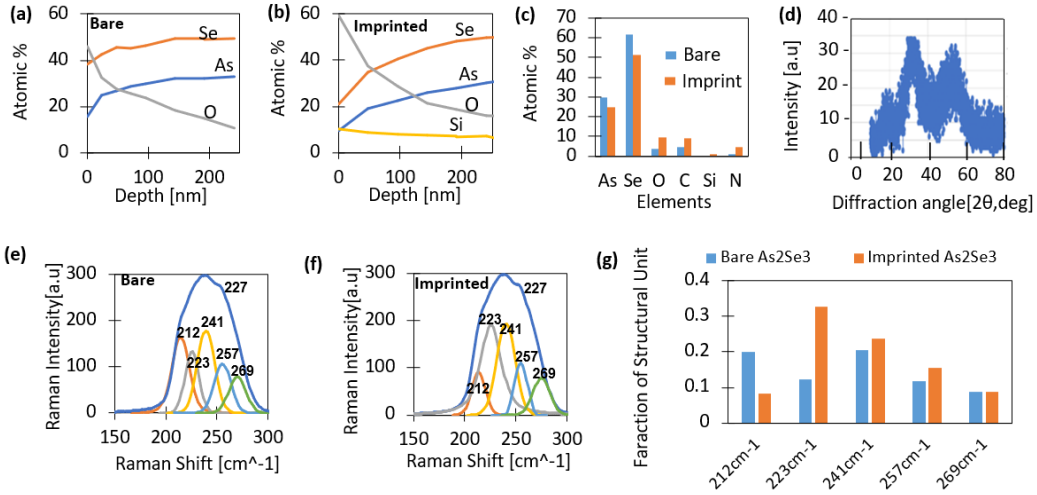

Fig. 3. Material analysis of bare and imprinted As_2Se_3. (a) and (b) XPS-based analysis of elements and different depths for bare and imprinted As_2Se_3, respectively. (c) EDS analysis of bare and imprinted As_2Se_3. (d) XRD of the imprinted sample, showing the amorphous structure of As_2Se_3. (e) and (f) Raman peaks of bare and imprinted substrates, respectively. (g) Fraction of Raman structural unit.

We also used Raman spectroscopy to estimate any possible effect of the imprinting process on the structure and composition of As_2Se_3. Figures 3(e),(f) show the Raman spectrum of bare and imprinted As_2Se_3, respectively. The deconvolution of the main Raman peak produced five peaks that correspond to different vibrational modes of As_2Se_3. These peaks are broad for both As_2Se_3 before and after the imprint, which provides additional confirmation that no crystallization took place during the imprinting process. Based on the areas of each peak, we also calculated the relative amounts of the structural units, in order to assess possible changes in material structure (Fig. 3(g)). In particular, the peak at 223 cm^{-1} corresponds to the vibration of As_2Se_3 pyramidal unit, and the increase in its area indicates the increase in the degree of crosslinking of the glass network. This observation mirrors previously reported Raman analysis of thermally imprinted As_2Se_3 thin films [17]. This increase in the cross- inking is the reason for the little decrease in the peak area related to the non-crosslinked units, such as the peak at 212 cm^{-1} that corresponds to As_4Se_4 unit. Overall, the surface analysis before and after the imprint clearly indicates that any changes in the material composition and structures caused by the imprinting are minor.

The demonstrated imprinting approach enables numerous optical applications of chalcogenide glasses that require surface patterning with functional microstructures. Here, we used this approach to realize antireflective moth-eye subwavelength structures designed for the mid-infrared spectrum. To that end, we first produced a master mold by self-assembly of 2 μm polystyrene microspheres into a dense monolayer on a silicon substrate using a Langmuir-Blodgett trough. The monolayer deposition was followed by the reduction of microsphere diameter in oxygen plasma (Corial DRIE 200L System, 100sccm O2, RF = 15W, LF = 200W, 30sec), Deep Reactive Ion Etching of silicon through the formed microsphere mask (Corial DRIE 200L, 36sccm SF_6, 15sccm C_2H_4, RF = 15W, LF = 250W, 15min), and the removal of the microspheres by washing in chlorobenzene. The obtained microstructures had a periodicity of 2 μm determined

Optics EXPRESS

by the initial microbead diameter, a height of ~1.2μm, and conical shapes with the top and bottom diameters of 1.35 and 1.75 microns, respectively (Fig. 4(a)). We then transferred the pattern from the master mold to a soft PDMS mold by casting standard PDMS-hardener mixture (1:10, Sylgard 184) on top of the master mold, curing it at 60°C for 1 hr, and peeling the hardened PDMS from the master surface, resulting in a negative 3D structure of the master mold (Fig. 4(b)). Finally, the obtained soft mold was used for the solvent-assisted imprinting as described above. Figure 4(c) shows an imprinted As_2Se_3 substrate, and Fig. 4(d) shows a high-resolution SEM image with the imprinted microstructures. Figure 4(e) presents an AFM image of the imprinted As_2Se_3, including 3D structure and cross-section. Both SEM and AFM images indicate that the dimensions of the imprinted microstructures, as well as their periodicity, are identical to those fabricated on the master mold. Most importantly, the measured height of the imprinted coni was 1.2 microns, which matches exactly the depth of the pits on the mold surface, indicating a perfect pattern transfer. Thus, it can be concluded that our imprinting process has a very high fidelity of pattern transfer not only for the nanoscale patterns, as shown previously, but also for patterns in the micron scale, which are particularly relevant for optical functionalities active in the infrared spectrum.

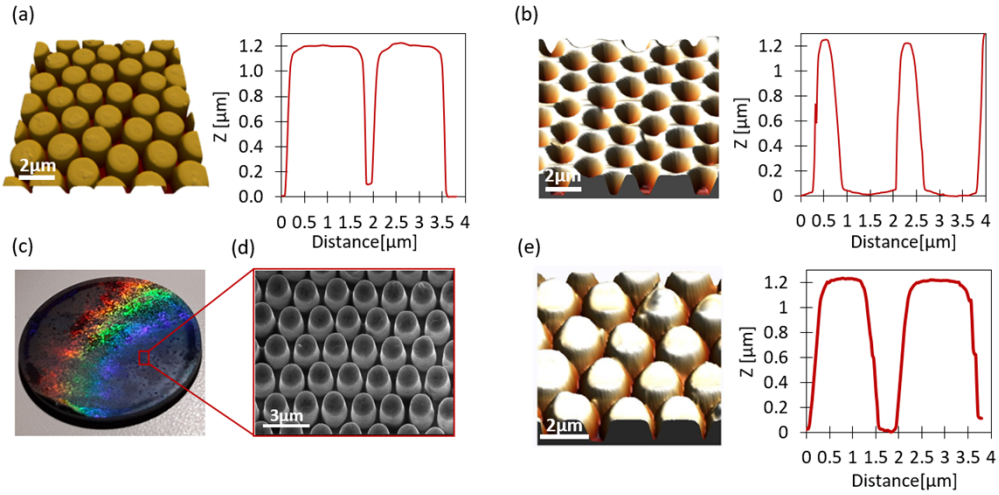

Fig. 4. Antireflective structure directly imprinted on As_2Se_3. (a),(b) AFM 3D scanning and x-section plot profile of the master mold and of soft mold used to imprint the structure, respectively. (c) Image of As_2Se_3 surface patterned with antireflective structure and SEM image of the structures on it. (e) AFM 3D scanning and x-section plot profile of the imprinted As_2Se_3 surface.

To demonstrate the optical functionality of the imprinted antireflective pattern, we measured its reflectance spectra at three different incident angles and compared them to those of a bare As_2Se_3 surface (Figs. 5(a)-(c)). It can be seen that while the bare As_2Se_3 reflects up to 25% of the incident light, the imprinted structures attenuated the reflection down to ~1%, which was observed at a spectral range of 6 to 7 microns for an incident angle of 11°. This achieved antireflective performance is comparable to that of moth-eye microstructures produced by a more complex and cumbersome imprint process than that reported before [22,23,25]. The measured spectrum is compared with a simulated spectrum, which was generated using Optilayer software package for each incidence angle, and took into account the experimental dimensions of the antireflective structures. It must be noted that the experimental spectrum shows a substantial attenuation in the reflection within the range much broader compared to the simulated spectrum. We believe that this broadband antireflective characteristic is due to the non-uniformity in height

Optics EXPRESS

of the antireflective structures across the sample. This non-uniformity is likely the reason beyond the observed blueshift of the experimentally obtained reflectance minima, as compared to the simulated ones. The experimental spectra also lack the interference peak that is clearly seen in the simulation at the wavelength of around 2 microns. Also, the experimental spectra represent the specular reflectance, which does not contain the effects of solid diffraction angles and scattering. These effects, however, are insignificant for the range of wavelength for which the antireflective microstructures were designed.

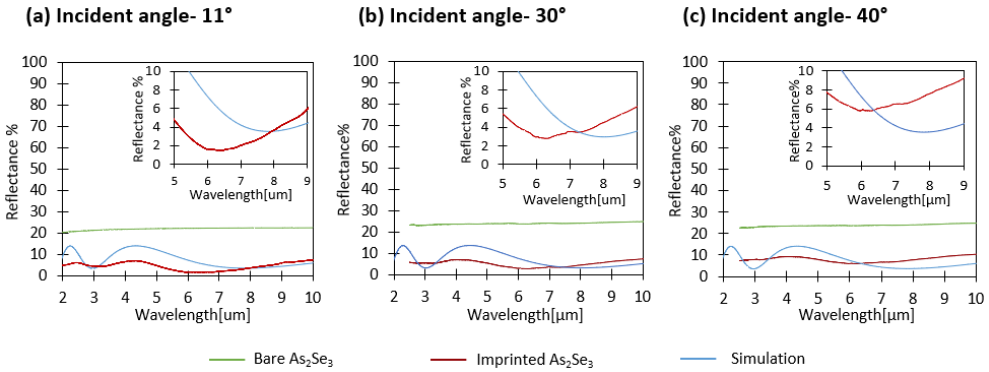

Fig. 5. Reflection spectra: Reflectance spectrum of surface imprinted with antireflective microstructures (red), compared to that of bare As_2Se_3 surface (green), and a simulated spectrum (blue) at an angle of (a) 11°, (b) 30°, (c) 40°. The inset shows the simulated and measured spectra in the range of 5–10 µm.

Finally, it is crucial to verify that the thermal imprinting of the surface does not produce the unwanted deformation of the imprinted substrate. To that end, we characterized surface flatness of both bare and imprinted As_2Se_3, using 3D laser scanner (Olympus, OLS5000, λ=630nm), and profilometer (Veeco Dektak Profilometer). The data is shown in Fig. 6. The profilometry shows that a pristine As_2Se_3 substrate has an initial bow of about 1.5 microns over 2 cm distance (which spans over almost the entire diameter of 1" sample), which likely stems from the shape of the preform used in its production. On the other hand, an imprinted As_2Se_3 substrate shows the same bow level. Also, the 3D surface scanning of the bare and imprinted substrates shows very similar levels of flatness, confirming that the demonstrated imprinting process does not produce any deformation of the substrate. This critical feature of our imprinting process is achieved due to the fact that the imprinting of a softened surface layer is done at a temperature significantly lower than that of the Tg of bare As_2Se_3, preventing its deformation.

In summary, we have demonstrated a novel, robust and facile approach for the direct nano-structuring of chalcogenide glasses. The ease of implementation of this approach stems from the standard PDMS-based soft mold commonly used for soft imprinting. By exploiting a hybrid mold version based on a hard imaging layer and soft support, we demonstrated that our approach is feasible for producing features down to 20 nm. On the other hand, we also demonstrated the fabrication of micron-scale features; therefore, this imprinting approach is highly versatile, it is not limited to a specific range of feature size and pattern resolutions, and can thus be applied to the fabrication of optical micro-/ nanostructures for a broad range of wavelengths, as well as a myriad of micro-nano structures whose applications are beyond optics. The robustness and high pattern fidelity of the demonstrated imprinting process are due to the softening of the surface layer of the imprinted chalcogenide glass. Yet, this softening also allows to achieve the additional important characteristic of this approach, which is the ability to imprint at a temperature below the glass transition point of pristine chalcogenide glass thereby maintaining the original shape of the directly imprinted substrate. Whereas previous methods of the direct imprint maintained

Optics EXPRESS

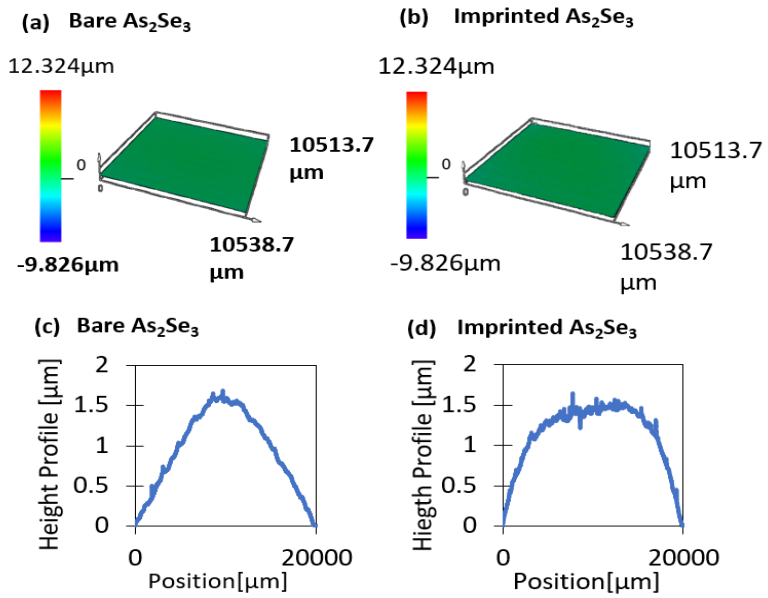

Fig. 6. Flatness measurements: (a),(b) 2D laser interferometry scan of the backside of the bare and imprinted As_2Se_3 substrates, respectively, showing that the surface was not deformed during the imprinting process; (c),(d) profilometry scans of bare and imprinted As_2Se_3 substrates showing similar levels of flatness.

the shape of the substrate by either complicated mechanical fixtures or complicated structural modification of the mold, our approach does so in a robust and straightforward way, without the need for a special equipment or specialized processes of mold fabrication. Overall, our approach is unique in its combination of three important features: (i) full pattern transfer for a broad range of feature sizes and resolution, (ii) complete conservation of the original substrate shape, and (iii) scalability and robustness of fabrication. As such, this paves the way to numerous applications that require direct patterning of chalcogenide glasses that have not been realizable up to date.

Funding. PAZY Foundation.

Disclosures. The authors declare no conflicts of interest.

Data availability. No data were generated or analyzed in the presented research.

References

1. L. Li, H. Lin, S. Qiao, Y. Zou, S. Danto, K. Richardson, J. D. Musgraves, N. Lu, and J. Hu, "Integrated flexible chalcogenide glass photonic devices," Nat. Photonics **8**(8), 643–649 (2014).
2. C. R. Petersen, U. Møller, I. Kubat, B. Zhou, S. Dupont, J. Ramsay, T. Benson, S. Sujecki, N. Abdel-Moneim, Z. Tang, D. Furniss, A. Seddon, and O. Bang, "Mid-infrared supercontinuum covering the 1.4–13.3 µm molecular fingerprint region using ultra-high NA chalcogenide step-index fibre," Nat. Photonics **8**(11), 830–834 (2014).
3. H. Lin, Y. Song, Y. Huang, D. Kita, S. Deckoff-Jones, K. Wang, L. Li, J. Li, H. Zheng, Z. Luo, H. Wang, S. Novak, A. Yadav, C.-C. Huang, R.-J. Shiue, D. Englund, T. Gu, D. Hewak, K. Richardson, J. Kong, and J. Hu, "Chalcogenide glass-on-graphene photonics," Nat. Photonics **11**(12), 798–805 (2017).
4. L. G. Aio, A. M. Efimov, and V. F. Kokorina, "Refractive index of chalcogenide glasses over a wide range of compositions," J. Non-Cryst. Solids **27**(3), 299–307 (1978).
5. G. B. Hoffman, W.-C. Liu, W. Zhou, R. Sooryakumar, P. Boolchand, and R. M. Reano, "Relief and trench formation on chalcogenide thin films using electron beams," J. Vac. Sci. Technol., B: Microelectron. Nanometer Struct.–Process., Meas., Phenom. **26**(6), 2478–2483 (2008).
6. E. V. Berlin, B. T. Kolomiets, V. M. Lyubin, S. I. Nesterov, V. V. Rudnev, and V. P. Shilo, "X-ray stimulated structural transformations in amorphous chalcogenide semiconductors," Sov. Tech. Phys. Lett **7**, 654–655 (1981).
7. M. Wuttig, H. Bhaskaran, and T. Taubner, "Phase-change materials for non-volatile photonic applications," Nat. Photonics **11**(8), 465–476 (2017).

Optics EXPRESS

8. H. Nasu, K. Kubodera, M. Kobayashi, M. Nakamura, and K. Kamiya, "Third-Harmonic Generation from Some Chalcogenide Glasses," J. Am. Ceram. Soc. **73**(6), 1794–1796 (1990).
9. V. S. Shiryaev and M. F. Churbanov, "Preparation of high-purity chalcogenide glasses," in *Chalcogenide Glasses* (Woodhead Publishing, 2014).
10. T. Zhou, Z. Zhu, X. Liu, Z. Liang, and X. Wang, "A Review of the Precision Glass Molding of Chalcogenide Glass (ChG) for Infrared Optics," Micromachines **9**(7), 337 (2018).
11. C. G. Bernhard and W. H. Miller, "A Corneal Nipple Pattern in Insect Compound Eyes," Acta Physiol. Scand. **56**(3–4), 385–386 (1962).
12. H. K. Raut, V. A. Ganesh, A. S. Nair, and S. Ramakrishna, "Anti-reflective coatings: A critical, in-depth review," Energy Environ. Sci. **4**(10), 3779–3804 (2011).
13. X. Li, J. He, and W. Liu, "Broadband anti-reflective and water-repellent coatings on glass substrates for self-cleaning photovoltaic cells," Mater. Res. Bull. **48**(7), 2522–2528 (2013).
14. K. C. Park, H. J. Choi, C. H. Chang, R. E. Cohen, G. H. McKinley, and G. Barbastathis, "Nanotextured silica surfaces with robust superhydrophobicity and omnidirectional broadband supertransmissivity," ACS Nano **6**(5), 3789–3799 (2012).
15. T. Han, S. Madden, D. Bulla, and B. Luther-Davies, "Low loss Chalcogenide glass waveguides by thermal nano-imprint lithography," Opt. Express **18**(18), 19286 (2010).
16. M. Solmaz, H. Park, C. K. Madsen, and X. Cheng, "Patterning chalcogenide glass by direct resist-free thermal nanoimprint," J. Vac. Sci. Technol., B: Microelectron. Nanometer Struct.–Process., Meas., Phenom. **26**(2), 606–610 (2008).
17. Y. Zou, D. Zhang, H. Lin, L. Li, L. Moreel, J. Zhou, Q. Du, O. Ogbuu, S. Danto, J. D. Musgraves, K. Richardson, K. D. Dobson, R. Birkmire, and J. Hu, "High-Performance, High-Index-Contrast Chalcogenide Glass Photonics on Silicon and Unconventional Non-planar Substrates," Adv. Opt. Mater. **2**(5), 478–486 (2014).
18. C. Tsay, Y. Zha, and C. B. Arnold, "Solution-processed chalcogenide glass for integrated single-mode mid-infrared waveguides," Opt. Express **18**(25), 26744 (2010).
19. J. Orava, T. Kohoutek, L. Greer, and H. Fudouzi, "Soft imprint lithography of a bulk chalcogenide glass," Opt. Mater. Express **1**(5), 796–802 (2011).
20. D. Yehuda, E. Kassis, S. Joseph, and M. Schvartzman, "Direct soft imprint of chalcogenide glasses," J. Vac. Sci. Technol., B: Nanotechnol. Microelectron.: Mater., Process., Meas., Phenom. **36**(3), 031602 (2018).
21. A. Pandey, S. Tzadka, D. Yehuda, and M. Schvartzman, "Soft thermal nanoimprint with a 10 nm feature size," Soft Matter **15**(13), 2897–2904 (2019).
22. M. R. Lotz, C. R. Petersen, C. Markos, O. Bang, M. H. Jakobsen, and R. Taboryski, "Direct nanoimprinting of moth-eye structures in chalcogenide glass for broadband antireflection in the mid-infrared," Optica **5**(5), 557 (2018).
23. M. Lotz, J. Needham, M. H. Jakobsen, and R. Taboryski, "Nanoimprinting reflow modified moth-eye structures in chalcogenide glass for enhanced broadband antireflection in the mid-infrared," Opt. Lett. **44**(17), 4383 (2019).
24. N. Ostrovsky, D. Yehuda, S. Tzadka, E. Kassis, S. Joseph, and M. Schvartzman, "Direct Imprint of Optical Functionalities on Free-Form Chalcogenide Glasses," Adv. Opt. Mater. **7**(19), 1900652 (2019).
25. S. Tzadka, N. Ostrovsky, E. Toledo, G. Le Saux, E. Kassis, S. Joseph, and M. Schvartzman, "Surface plasticizing of chalcogenide glasses: a route for direct nanoimprint with multifunctional antireflective and highly hydrophobic structures," Opt. Express **28**(19), 28352–28365 (2020).
26. T. W. Odom, J. C. Love, D. B. Wolfe, K. E. Paul, and G. M. Whitesides, "Improved pattern transfer in soft lithography using composite stamps," Langmuir **18**(13), 5314–5320 (2002).
27. M. Rosenberg and M. Schvartzman, "Direct Resistless Soft Nanopatterning of Freeform Surfaces," ACS Appl. Mater. Interfaces **11**(46), 43494–43499 (2019).
28. S. Song, J. Dua, and C. B. Arnold, "Influence of annealing conditions on the optical and structural properties of spin-coated As_2S_3 chalcogenide glass thin films," Opt. Express **18**(6), 5472–5480 (2010).